The development of a nonstationary standardised streamflow index using climate and reservoir indices as covariates

Menghao Wang[a, b], Shanhu Jiang[a, b*], Liliang Ren[a, b], Chong-Yu Xu[c], Linyong Wei[b], Hao Cui[b], Fei Yuan[b], Yi Liu[b], Xiaoli Yang[b]

[a]*State Key Laboratory of Hydrology-Water Resources and Hydraulic Engineering, Hohai University, Nanjing 210098, China*

[b]*College of Hydrology and Water Resources, Hohai University, Nanjing 210098, China*

[c]*Department of Geosciences, University of Oslo, Oslo, Norway*

Submit to *Water Resource Management*

*Corresponding author: Shanhu Jiang

State Key Laboratory of Hydrology-Water Resources and Hydraulic Engineering, Hohai University, Nanjing 210098, China

Email: hik0216@hhu.edu.cn

1 **Abstract**

2   Under current global change, the driving force of evolution of drought has

3 gradually transitioned from a single natural factor to a combination of natural and

4 anthropogenic factors. Therefore, widely used standardised drought indices based on

5 assumption of stationarity are challenged and may not accurately assess characteristics

6 of drought processes. In this study, a nonstationary standardised streamflow index

7 (NSSI) that incorporates climate and reservoir indices as external covariates was

8 developed to access nonstationary hydrological drought. The first step of the proposed

9 approach is to apply methods of trend and change point analysis to assess the

10 nonstationarity of streamflow series to determine type of streamflow regime, that is, the

natural and altered regime. Then, different nonstationary models were constructed to calculate the NSSI by selecting climate indices as covariates for streamflow series with natural regime, and climate and reservoir indices as covariate for streamflow series with altered regime. Four stations in the upper reaches of the Huaihe River basin, China, were selected to examine the performance of the proposed NSSI. The results indicated that Dapoling (DPL), Changtaiguan (CTG), and Xixian (XX) stations had natural streamflow regimes, while the Nanwan (NW) station had an altered regime. The global deviances of the optimal nonstationary models were 17 (2.2%), 18 (2.9%), 26 (4.0%), and 22 (3.5%) less than those of stationary models for DPL, CTG, NW, and XX stations, respectively. Especially, for the NW station influenced by reservoir regulations, the frequency of slight drought and moderate drought of NSSI was 12.8% lower than and 13.1% greater than those of SSI, respectively. Overall, the NSSI that incorporates the influence of climate variability and reservoir regulations provided more reliable assessment of hydrological drought than the traditional SSI.

Keywords: Hydrological drought; Nonstationary standardised streamflow index; Climate variability; Reservoir regulation

1. Introduction

Droughts are regarded as complex and multidimensional phenomena that pose a threat to water security worldwide (Araghinejad 2011; Ali et al. 2021; Wang et al. 2021). Traditionally, droughts are classified into four categories, including meteorological, agricultural, hydrological, and socioeconomic drought (David and Davidová 2017; AghaKouchak et al. 2021). As an important form of drought, hydrological drought can cover extensive areas and can last for months to years (Van Loon 2015). For example,

36   in 2014, the state of California in the USA faced one of the most severe multiyear

37   droughts on record, resulting in extremely low reservoir and groundwater levels

38   (Aghakouchak et al. 2014). Therefore, accurate understanding and quantification of

39   hydrological droughts are essential for water management and policy making.

40   Several hydrological drought indices have been proposed over the past few

41   decades and they are generally divided into two groups—standardised indices and

42   threshold-based indices. The most widely used standardised indices are the

43   standardised runoff index (SRI; Shukla and Wood 2008) and the standardised

44   streamflow index (SSI; Vicente-Serrano et al. 2012). Both indices have a calculation

45   procedure similar to standardised precipitation index (SPI), which involves fitting a

46   probability distribution to a hydrological variable and transforming the distribution to

47   a normal distribution. Another method for deriving hydrological drought events is the

48   threshold level method (Van loon and Van Lanen 2013). This approach sets a pre-

49   defined threshold level, and when the target variable (e.g., streamflow) is below this

50   level, the site is considered to be in a state of drought.

51   Traditionally, drought indices are calculated based on the fundamental assumption

52   of statistical stationarity and assumed that the probabilistic characteristics of the hydro-

53   meteorological process do not change over time. However, Milly et al (2008) argued

54   that the effects of climate change and anthropogenic activities challenge the

55   fundamental assumption of stationarity. Thus, in a changing environment, alternative

56   approaches should be developed to consider nonstationarity and allow probabilistic

57   parameters to change over time (Salas and Obeysekera 2014). In this way, statistical

58   distribution parameters are expressed as functions of covariates to model

59   nonstationarity generated by climatic and anthropogenic impacts.

60   Several studies have attempted to consider the impact of nonstationarity on the

61 evaluation of hydrological droughts. Zou et al (2018) used the generalised additive

62 model for location, scale, and shape (GAMLSS) to construct a time-dependent SRI

63 (SRI_{var}), with its parameters linked with time to fit a long-term streamflow time series,

64 to assess the impacts of climate change and human activities on hydrological drought.

65 However, many studies have indicated that nonstationary models in which the

66 parameters vary only with time cannot adequately capture the variability of hydro-

67 meteorological variables (Wang et al. 2021c). In recent years, many researchers have

68 emphasised that choosing large-scale climate indices as covariates of streamflow in

69 nonstationary models would better characterise the nonstationarity caused by climate

70 variability (Forootan et al. 2019). In addition to climate variability, human activity is

71 another driver of nonstationarity (Jiang et al. 2019). Among diverse anthropogenic

72 activities (e.g., irrigation, dams and reservoirs, and inter-basin water transfer), reservoir

73 construction and regulation usually cause the greatest shifts in flow regimes (Slater et

74 al. 2021). Some recent studies have attempted to parameterise the influence of reservoir

75 construction and regulation to investigate the resulting nonstationary impacts on

76 streamflow processes. For example, López and Francés (2013) carried out

77 nonstationary flood frequency analysis for continental Spanish rivers using climate and

78 reservoir indices (RI) as external covariates. Jiang et al. (2015) selected time and RI as

79 covariates to explore how reservoirs altered low-flows. However, research on

80 nonstationary hydrological drought assessment with the incorporation of climate

81 variability and anthropogenic reservoir regulations remains limited.

82   Here, we develop a nonstationary standardised streamflow index (NSSI) using the

83 GAMLSS, with its parameters vary nonlinearly with climate indices and RI. The

84 specific objectives of the study were to (1) use trend and change point analysis methods

85 to reveal the nonstationarity of streamflow series under the impacts of climate

86   variability and reservoir regulations; (2) select the most significant climate indices and

87   calculate the RI for use as covariates to construct the NSSI based on the GAMLSS

88   model; and (3) compare the NSSI with the traditional SSI in the evaluation of

89   hydrological drought to assess the efficiency of the NSSI. The Xixian basin, located in

90   the upper reaches of the Huaihe River Basin, China, was chosen as a case study to

91   evaluate the developed NSSI. The NSSI is expected to provide a useful tool for the

92   evaluation of nonstationary hydrological drought in a changing environment.

93

94   **2. Study area and data**

95   2.1 Study area

96   The Xixian basin, located in the upper reaches of the Huaihe River Basin in eastern

97   China (31.5 °N–32.75 °N, 113.25 °E–115 °E), covers an area of 10,191 km^2 (Fig. 1). The

98   basin is situated in the transition zone of mid-latitude humid and semi-arid climates

99   (Jiang et al. 2020), and both flood and hydrological drought events occur frequently.

100   We selected Dapoling, (DPL), Changtaiguan (CTG), Nanwan (NW), and Xixian (XX)

101   stations as the case study areas. Several studies have indicated that three large reservoirs

102   (i.e., Nanwan, Feishahe, and Huashan reservoirs in Fig. 1) have impacts on hydrological

103   extremes (e.g., hydrological drought) in the study area (Shi et al. 2011).

104

105   2.2 Data

106   The observed monthly precipitation of the 35 rain-gauge stations and streamflow

107   of the four hydrological stations during 1955–2016, and information of three large

108   reservoirs in the upper reaches of NW station were obtained from the Hydrological

109   Bureau of the Ministry of Water Resources of China. Capacity and completion date of

110   the Nanwan, Feishahe, and Huashan reservoirs were 1630, 82, 173 million m^3 and 1955,

111   1961, 1967, respectively. According to previous studies (Ouyang et al. 2014), six large-

112   scale climate indices with proven influence on the streamflow of Xixian basin, i.e., AO,

113   AMO, NAO, PDO, NPO, and ENSO were selected as candidate covariates. They were

114   obtained from the National Oceanic and Atmospheric Administration (NOAA)

115   Physical Sciences Laboratory website (https://psl.noaa.gov/data/climateindices/).

116

117   **3. Methods**

118   The framework of the proposed NSSI consisted of three steps as shown in Fig. 2.

119   (1) Nonstationary analysis of hydro-meteorological variables; (2) Construction of the

120   NSSI; and (3) Validation of the NSSI. The methods used in this study are described in

121   detail in following sections.

122

123   3.1 Nonstationary analysis methods

124   The robustness of the traditional Mann-Kendall (MK) trend test is usually

125   influenced by the persistence of the hydro-meteorological series. To improve the MK

126   test method, Hamed and Rao (1998) used *lag-i* autocorrelation to remove persistence

127   and make the test more robust, known as the modified Mann-Kendall (MMK) trend test.

128   In this study, we used the MMK method to identify trends of the hydro-meteorological

129   series.

130   Conventional statistical test methods for identification of change points such as

131   Mann-Kendell test and sliding T test are usually based on the assumption that the time

132   series should be linear and stationary. However, it is difficult for them to accurately

133   capture the change points in the nonlinear or nonstationary time series. To make up this

134   shortcoming, this study applied the heuristic segmentation method, proposed by

135   Bernaola-Galvan et al. (2001), to identify change points in nonlinear and nonstationary

136   series. In addition, the precipitation-streamflow double cumulative curve (DCC)

137   method was also applied to identify change points. Generally, a change in the gradient

138   of the curve implies that the characteristics of precipitation or streamflow may have

139   changed, and the inflection point of the curve is generally regarded as a change point

140   (Wang et al. 2020b).

141

142   3.2 Calculation of the NSSI

143   A 3-month SSI (SSI-3) will not cause the SSI value to change too fast or too slowly.

144   Therefore, SSI-3 (Vicente-Serrano et al. 2012) was considered more suitable for the

145   identification of continuous drought events in the Xixian basin. In this study, the

146   drought grades can be divided into five classes based on the SRI values: non-drought

147   when SRI > –0.5, slight drought (D1) when –1.0 < SRI ≤ –0.5, moderate drought (D2)

148   when –1.5 < SRI ≤ –1.0, severe drought (D3) when –2.0 < SRI ≤ –1.5, and extreme

149   drought (D4) when SRI ≤ –2.0. Besides, a stationary model (M1) and a nonstationary

150   model (M2) were developed to calculate SSI and NSSI, respectively. In M1, a

151   streamflow series was fitted to a stationary model with constant distribution parameters

152   to construct a stationary SSI series. In M2, a streamflow series was fitted to a

153   nonstationary model based on the GAMLSS model with distribution parameters

154   varying with climate indices and/or the RI to construct a NSSI series. The main steps

155   to construct the NSSI includes: (1) selection of significant climate indices and

156   calculation of RI; and (2) non-stationary probability fitting of streamflow based on

157   GAMLSS model and calculation of the NSSI.

158

159   3.2.1 Selection of significant climate indices

160   To reduce the monthly random variability (Wang et al. 2020c) and maintain

161 consistency with NSSI-3 (or SSI-3), each climate index was processed using a 3-month

162 moving average. With regard to the streamflow series in a specified month, the

163 reconstructed time series considering lead times of 1-, 2-, ..., 12-months were prepared

164 for the correlation analysis. Kendall's rank correlation test was performed at the 95%

165 confidence level to identify significant climate indices that can be considered covariates

166 to fit the streamflow records in the nonstationary model.

167

168 3.2.2 Calculation of the RI

169 The dimensionless RI proposed by López and Francés (2013) is an effective

170 indicator to reflect the impact of reservoir construction on flow regimes. It is calculated

171 as follows:

172 $$RI = \sum_{i=1}^{N} \left(\frac{A_i}{A_T} \right) \cdot \left(\frac{C_i}{C_T} \right) \tag{1}$$

173 where N is the number of reservoirs upstream of the gauge station, A_i is the catchment

174 area of each reservoir, A_T is the catchment area of the gauge station, C_i is the total

175 capacity of each reservoir, and C_T is the mean annual streamflow at the gauge station.

176 The RI threshold value between low and high alteration was found to be 0.25, and the

177 higher the RI value, the greater the reservoir influence.

178

179 3.2.3 GAMLSS

180 The GAMLSS proposed by Rigby and Stasinopoulos (2005) assumed that

181 independent observations x_i for i =1, 2, 3, ..., n have the distribution function $f(x_i \mid \theta^i)$

182 where $\theta^i = (\theta_1^i, \theta_2^i, ..., \theta_p^i)$ is a vector of p distribution parameters accounting for the

183 location, scale, and shape random variable characteristics. The distribution parameters

184 are related to covariates by the monotonic link functions $g_k(\cdot)$ for k = 1, 2, ..., p, where

185   the parameters are modelled through proper link functions:

186
$$g_k\left(\theta_k\right)=\eta_k=X_k\beta_k+\sum_{j=1}^{J_k}Z_{jk}x_{jk} \tag{2}$$

187   where η_k and θ_k are vectors of length n, for example $\theta_k^T=\left(\theta_k^1,\theta_k^2,\cdots,\theta_k^n\right)$; X_k is a matrix

188   of explanatory variables (i.e., covariates) of order $n\times J_k$; $\beta_k^T=\left(\beta_{1k},\beta_{2k},\cdots,\beta_{J_kk}\right)$ is a

189   parameter vector of length J_k; Z_{jk} is a fixed known $n\times q_{jk}$ design matrix; and x_{jk} is a q_{jk}-

190   dimensional random variable.

191   In this study, we selected six widely used two-parameter continuous distributions

192   to fit the streamflow data, including the Weibull, Gumbel, Gamma, Logistic, Normal,

193   and Lognormal distributions (Vicente-Serrano et al. 2012; Wang et al. 2020a). The

194   model that achieved the minimum Global deviance (GD), Akaike information criterion

195   (AIC), and Schwarz Bayesian information criterion (BIC) values was selected as the

196   optimal nonstationary model. A visual inspection of the diagnostic plots of the residuals

197   (i.e., worm plot) was also used to ensure that the selected model adequately described

198   the systematic part of each time series. All calculations were performed using the R

199   platform and the freely available '*gamlss*' package. Mathematically, the calculation of

200   the NSSI is similar to that of the SSI but is based on the selected optimal nonstationary

201   models. The classification of drought grades for the NSSI is the same as that of the SSI.

202

203   3.3 Copula and joint return period

204   In this study, we selected the "and ($\cap$)" joint return period (Salvadori and De

205   Michele 2004) to calculate the joint probability (P_{DS}) and joint return period (T_{DS}) of

206   drought duration and severity:

207
$$P_{DS}=P(D\ge d,S\ge s)=1-F_D(d)-F_S(s)+C(F_D(d),F_S(s)) \tag{3}$$

9 / 28

208
$$T_{DS} = \frac{E(L)}{P(D \geq d \cap S \geq s)} = \frac{E(L)}{1 - F_D(d) - F_S(s) + C(F_D(d), F_S(s))}$$
(4)

209 where $C(F_D(d), F_S(s))$ is the joint distribution of drought duration and severity, and $E(L)$

210 represents the average time interval of drought events.

211 The six continuous distributions in section 3.2.3 were selected to determine the

212 optimal marginal distribution of the drought severity series. Two widely used discrete

213 distributions namely the Negative Binomial and Poisson distributions were applied to

214 fit the drought duration series. The distribution that showed the smallest d value, as

215 calculated by the Kolmogorov-Smirnov (K-S) test, was selected as the optimal marginal

216 distribution. Then, the optimal copula function was selected from five commonly used

217 theoretical copula functions, namely the Gaussian-copula, T-copula, Clayton-copula,

218 Frank-copula, and Gumbel-copula functions (Wang et al. 2020a).

219

220 **4. Results**

221 4.1 Nonstationary analysis of hydro-meteorological series

222 Figs. 3(a)-(b) show that the seasonal distributions of precipitation of the four

223 stations are consistent, with most of the precipitation falling between May and

224 September. Streamflow of the NW station peaks in and concentrated around June, while

225 that of the other stations peak in and concentrated around July. DCCs of the Figs. 3(c)-

226 (f) illustrate that precipitation and streamflow of the DPL, CTG, and XX stations

227 remained consistent, whereas this relationship of the NW station had been disturbed

228 since 1956. Table 1 shows that streamflow of the NW station showed a significant

229 download trend ($\alpha < 0.05$). Heuristic segmentation test identified two significant change

230 points ($\alpha < 0.05$) of the NW station in 1956 and 1967, respectively. According to these

231 results, the DPL, CTG, and XX stations can be considered as stations with a 'natural'

232 streamflow regime and the NW station can be selected as a station with a 'altered'

233   streamflow regime.

234

235   4.2 Construction of the NSSI

236   Table 2 shows the identification results of significant climate indices in CTG

237   station. The results indicated that ENSO was selected as the significant index in January

238   to February and August to December; NPO was regarded as a crucial impact factor for

239   streamflow in March, April, June, and October to December; PDO dominantly affected

240   streamflow in August to November; AMO was selected as the significant climate index

241   in all the months. Besides, the maximum RI values (i.e., nowadays) were 0.0014,

242   0.0012, 0.3203, and 0.0049 for DPL, CTG, NW, and XX stations, respectively. The RI

243   value of the NW station was larger than the threshold (i.e., 0.25), while that of the other

244   stations was far less than 0.25. Figs. 3 (g), (h), and (j) show that for stations with a low

245   RI, reservoir construction had less impact on the streamflow regime. However, for the

246   NW station with a high RI value (Fig. 3 (i)), the streamflow regime has been strongly

247   altered since 1967. Therefore, for stations with natural regimes, significant climatic

248   indices should be considered when building nonstationary models. For the NW station,

249   alongside climatic indices, the RI will also be considered as an external covariate.

250   Table 3 shows that the all the GD, AIC, and BIC values of M2 were smaller than

251   those of M1 in all the 12 months at NW station. The GD of M2 was reduced by 9 (1.2%

252   in July) to 28 (4.4% in April) compared with M1. Table 4 shows that the Lognormal

253   distribution (LOGNO) gave the best fits for the three natural stations, and the Logistic

254   distribution (LO) gave the best fit for the altered NW station. The average GDs of M2

255   model were 17 (2.2%), 18 (2.9%), 26 (4.0%), and 22 (3.5%) less than those of M1

256   model for DPL, CTG, NW, and XX stations, respectively.

257   Fig. 4 shows that M2 performed better than M1 when describing the variability of

258   the streamflow series in normal (March), wet (June), and dry (December) months. For

259   example, in normal month (Fig. 4(a)), the area spanned by the 5th and 95th quantiles

260   of M1 covered 94%, 90%, 89% and 94% of the observed points at the four stations.

261   Whereas that of M2 covered 98%, 98%, 94% and 97% of the observed points,

262   respectively. Fig. 5 shows that all residual points of M1 and M2 for the three natural

263   stations fell within the 95% confidence intervals. However, the residual values of the

264   NW station for M1 (Fig. 5 (c)) shows deviations from normality, while those of M2

265   (Fig. 5 (g)) do not show a departure from normality. Therefore, the nonstationary M2

266   that incorporated climate indices and RI as covariates can evidently provide a better fit

267   for streamflow series. Then, the optimal M2 models were used to fit the streamflow

268   data and to calculated the NSSI series.

269

270   4.3 Validation of the NSSI

271   According to the historical records (Chinese Office of State Flood Control and

272   Drought Relief Headquarters, OSFCDRH 1997), two historical drought events that

273   occurred in 1978–1979 and 1993 at the NW station were chosen to examine the

274   performance of the NSSI and SSI. The extreme droughts 1978–1979 (the first gray

275   shadow bars in Fig. 6(a)) caused a serious reduction in crop production in the Xixian

276   basin. The NSSI captured an extreme hydrological drought event from August 1978 to

277   April 1980, which reached the most (i.e., –2.65) in September 1979. Whereas, the SSI

278   values during this period were all below the level of severe drought (i.e., SSI > –2). In

279   1993, a hydrological drought event occurred from spring to autumn in NW station (the

280   second gray shadow bars in Fig. 6(a)), among which drought in autumn had the greatest

281   impact (Zhu et al. 2016). NSSI index captured the gradual aggravation trend of this

282   hydrological drought event from spring to autumn, while the drought process captured

283 by SSI had been maintained at the level of moderate drought (i.e., SSI > –1.5).

284   Fig. 6(d) shows that the frequency of slight (D1) and moderate (D2) drought of

285 NSSI of the NW station were 12.8% lower and 13.1% greater than that of SSI,

286 indicating that reservoir regulations in the upper reach of the NW station caused more

287 slight droughts developed into moderate droughts. Besides, Negative Binomial (NB)

288 and LOGNO distributions were the optimal marginal distribution functions for drought

289 duration and severity of the four stations, respectively. Frank-copula function was the

290 optimal copula functions for the joint distribution of drought duration and severity of

291 these stations. Figs. 6(f)-(m) show that joint contour plots of the NSSI (M2) were

292 moving forward in comparison with those calculated from the SSI (M1), indicating that

293 the drought risk identified by the NSSI series is increased compared with that of SSI

294 series.

295

296 **5. Discussion**

297   The traditional SSI is widely used for hydrological drought assessment and it is

298 generated by fitting streamflow series to a distribution with constant parameters based

299 on stationary assumption (Wang et al., 2020c). However, effects of climate variability

300 and anthropogenic activities challenge the fundamental assumption of stationarity, and

301 statistical distribution parameters may change with these forcing factors (Jiang et al.

302 2015). In this study, the proposed NSSI were generated from probability models that

303 distribution parameters varying with significant climate indices and RI, thus providing

304 an effective tool for nonstationary hydrological drought assessment. On the one hand,

305 comparisons of criteria values, i.e., the GD, AIC, and BIC between M1 and M2 (Tables

306 3 and 4) showed that nonstationary models had smaller fitting residuals. Centile curves

307 and worm plots (Figs.4 and 5) showed that model M2 provided a better description of

308   streamflow processes than M1. On the other hand, the verification results (Fig. 6)

309   showed that the NSSI that incorporate the climate variability and reservoir regulations

310   will give a more reliable description of drought condition and process.

311   Climate variability is widely recognised as one of the most important multi-years

312   to multi-decadal drivers of changes in hydro-climatic extremes (Slater et al. 2021). As

313   shown in Fig. 4, the nonstationary models considering different lead times when

314   selecting the climate indices were better at describing streamflow and drought

315   conditions. Such attempts will contribute to a deeper understanding of historical

316   hydrological drought events at catchment and regional scales (Van Loon 2015). More

317   importantly, the advantage of employing climate variability is that climate model

318   predictions can be employed as covariates to estimate future changes in drought

319   processes (Slater et al. 2021). In addition, with the increase in global population and

320   the growing demand for water, anthropogenic impacts on surface hydrological

321   processes have greatly increased (AghaKouchak et al. 2014, 2021). Among diverse

322   anthropogenic water use activities, reservoir regulations usually have a more direct

323   influence on flow regimes (Slater et al. 2021). The Figs. 4-6 revealed that for the NW

324   station, the nonstationary models considering the RI as a covariate provided a more

325   accurate fit of the streamflow data, especially changes occurring before and after

326   streamflow change points related to reservoir construction. Such attempts provide an

327   idea for parameterizing the human influence and then applying it as covariates to

328   construct a nonstationary standard streamflow index.

329   Finally, some limitations should be emphasized is that the proposed NSSI in this

330   study only considered the nonstationarity caused by climate variability and reservoir

331   regulation. When the NSSI is applied to other regions, other nonstationary forcing

332   factors should be considered, such as land use and cover change, irrigation, and

333　abstraction (AghaKouchak et al. 2021; Slater et al. 2021). The future work could focus

334　on developing some parameterisation schemes that can account for human activities

335　and then applying them to the NSSI construction framework.

336

337　**6. Conclusions**

338　　In this study, we developed a NSSI that incorporates large-scale climate indices

339　and the RI as external covariates based on the GAMLSS model. The large-scale climate

340　indices were selected based on correlation analysis to represent impacts of climate

341　variability, and the RI was calculated to represent influence of anthropogenic reservoir

342　regulation. As such, our comprehensive consideration of the nonstationary impacts of

343　these factors on hydrological drought assessment is the innovative part of this research.

344　　We demonstrated the application of the developed NSSI to the Xixian basin

345　located in the upper reaches of the Huaihe River Basin, China. For this basin, the

346　average GDs of M2 model were 17 (2.2%), 18 (2.9%), 26 (4.0%), and 22 (3.5%) less

347　than those of M1 model for DPL, CTG, NW, and XX stations, respectively, indicating

348　that the nonstationary models performed better than stationary model in describing the

349　nonstationary streamflow processes. Especially, for the NW station, the frequency of

350　slight drought and moderate drought of NSSI was 12.8% lower than and 13.1% greater

351　than those of SSI, respectively. These revealed that the NSSI can correctly capture the

352　variations of hydrological drought due to influence of reservoir regulations.

353　　Overall, the developed NSSI in this study provides an appropriate method for

354　assessing nonstationary hydrological droughts in a changing environment. Such

355　attempts are expected to provide a valuable reference for nonstationary drought

356　research in other regions as well as the development of new drought assessment

357　methods.

Author Contribution

Conceptualization: Menghao Wang; Methodology: Linyong Wei, Hao Cui, Fei Yuan, Yi Liu, and Xiaoli Yang; Funding acquisition: Shanhu Jiang, Liliang Ren, and Chong-Yu Xu.

Data Availability

The data that support the findings of this study are openly available at https://www.usgs.gov/ and https://psl.noaa.gov/data/climateindices/.

Declarations

Ethical Approval

Not applicable.

Consent to Participate

Not applicable.

Consent to Publication

Not applicable.

Competing Interests

The authors declare that they have no competing interests.

References

Aghakouchak A, Feldman D, Stewardson M, et al (2014) Australia's drought: lessons for California. Science, 343(6178), 1430-1431.

AghaKouchak A, Mirchi A, Madani K, et al (2021) Anthropogenic Drought: Definition, Challenges, and Opportunities. Rev Geophys 59:1–23.

Ali Z, Ellahi A, Hussain I, et al (2021) Reduction of Errors in Hydrological Drought Monitoring – A Novel Statistical Framework for Spatio-Temporal Assessment of Drought. Water Resour Manag 35:4363–4380.

Araghinejad S (2011) An Approach for Probabilistic Hydrological Drought Forecasting. Water Resour Manag 25:191–200.

Bernaola-Galván P, Ivanov PC, Nunes Amaral LA, Stanley HE (2001) Scale invariance in the nonstationarity of human heart rate. Phys Rev Lett 87:1–4.

Chinese Office of State Flood Control and Drought Relief Headquarters (OSFCDRH) (1997) Floods and Droughts in China. China Water & Power Press, Beijing (in Chinese).

David V, Davidová T (2017) Relating hydrological and meteorological drought indices in order to identify causes of low flows in the catchment of blanice river. Environ Process 4:149–161.

Forootan E, Khaki M, Schumacher M, et al (2019) Understanding the global hydrological droughts of 2003–2016 and their relationships with teleconnections. Sci Total Environ 650:2587–2604.

Hamed KH, Ramachandra Rao A (1998) A modified Mann-Kendall trend test for autocorrelated data. J Hydrol 204:182–196.

Jiang C, Xiong L, Xu CY, Guo S (2015) Bivariate frequency analysis of nonstationary low-flow series based on the time-varying copula. Hydrol Process 29:1521–1534.

Jiang S, Liu R, Ren L, et al (2020) Evaluation and Hydrological Application of CMADS Reanalysis Precipitation Data against Four Satellite Precipitation Products in the Upper Huaihe River Basin, China. J Meteorol Res 34:1096–1113.

Jiang S, Wang M, Ren L, et al (2019) A framework for quantifying the impacts of climate change and human activities on hydrological drought in a semiarid basin of Northern China. Hydrol Process 33:1075–1088.

López J, Francés F (2013) Non-stationary flood frequency analysis in continental Spanish rivers, using climate and reservoir indices as external covariates. Hydrol Earth Syst Sci 17:3189–3203.

Milly PCD, Betancourt J, Falkenmark M, et al (2008) Climate change: Stationarity is dead: Whither water management? Science 319:573–574.

Ouyang R, Liu W, Fu G, et al (2014) Linkages between ENSO/PDO signals and precipitation, streamflow in China during the last 100 years. Hydrol Earth Syst Sci 18:3651–3661.

Rigby RA, Stasinopoulos DM, Lane PW (2005) Generalized additive models for location, scale and shape. J R Stat Soc Ser C Appl Stat 54:507–554.

Salas JD, Obeysekera J (2014) Revisiting the Concepts of Return Period and Risk for Nonstationary Hydrologic Extreme Events. J Hydrol Eng 19:554–568.

Salvadori G, De Michele C (2004) Frequency analysis via copulas: Theoretical aspects and applications to hydrological events. Water Resour Res 40:1–17.

Shi P, Chen C, Srinivasan R, et al (2011) Evaluating the SWAT Model for Hydrological Modeling in the Xixian Watershed and a Comparison with the XAJ Model. Water Resour Manag 25:2595–2612.

Shukla S, Wood AW (2008) Use of a standardized runoff index for characterizing hydrologic drought. Geophys Res Lett 35:1–7.

Slater LJ, Anderson B, Buechel M, et al (2021) Nonstationary weather and water extremes: A review of methods for their detection, attribution, and management. Hydrol Earth Syst Sci 25:3897–3935.

Van Loon AF, Van Lanen HAJ (2013) Making the distinction between water scarcity and drought using an observation-modeling framework. Water Resour Res 49:1483–1502.

Van Loon AF (2015) Hydrological drought explained. WIREs Water 2:359–392.

Vicente-Serrano SM, López-Moreno JI, Beguería S, et al (2012) Accurate Computation of a Streamflow Drought Index. J Hydrol Eng 17:318–332.

Wang F, Wang Z, Yang H, et al (2020a) Comprehensive evaluation of hydrological drought and its relationships with meteorological drought in the Yellow River basin, China. J Hydrol 584.

Wang M, Jiang S, Ren L, et al (2020b) An approach for identification and quantification of hydrological drought termination characteristics of natural and human-influenced series. J Hydrol 590.

Wang M, Jiang S, Ren L, et al (2021) Separating the effects of climate change and human activities on drought propagation via a natural and human-impacted catchment comparison method. J Hydrol 603.

Wang Y, Duan L, Liu T, et al (2020c) A Non-stationary Standardized Streamflow Index for hydrological drought using climate and human-induced indices as covariates. Sci Total Environ 699.

Zhu Y, Wang W, Singh VP, Liu Y (2016) Combined use of meteorological drought indices at multi-time scales for improving hydrological drought detection. Sci Total Environ 571:1058–1068.

Zou L, Xia J, She D (2018) Analysis of Impacts of Climate Change and Human Activities on Hydrological Drought: A Case Study in the Wei River Basin, China. Water Resour Manag 32:1421–1438.

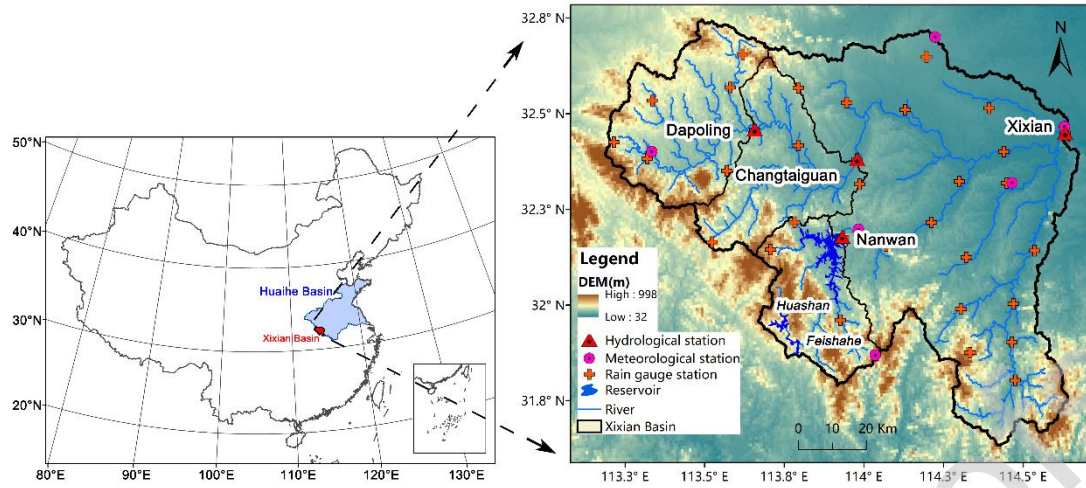**Fig. 1.** Location of the study area and the distribution of hydrological and rain gauge stations and reservoirs.
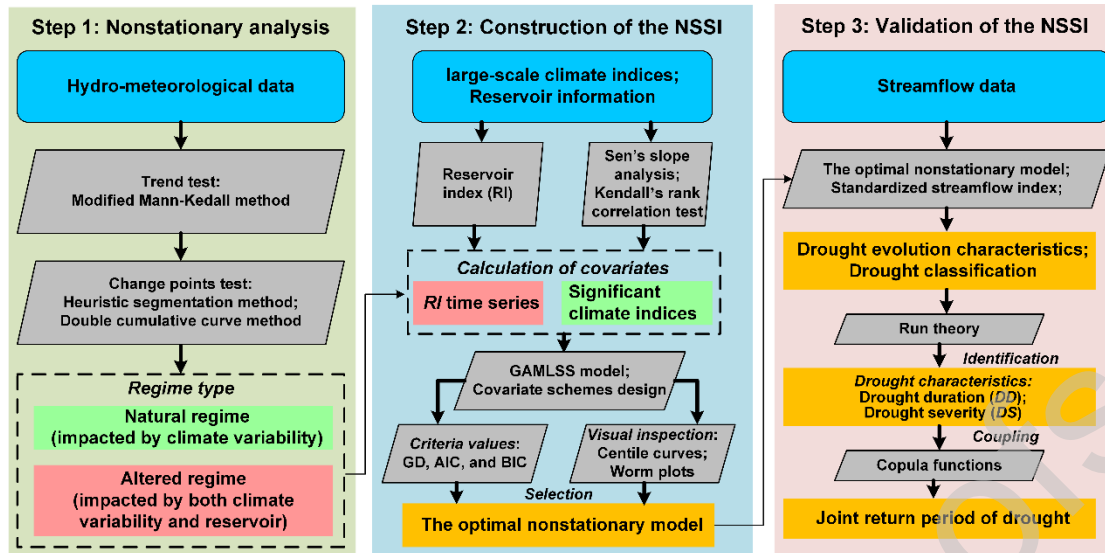
Fig. 2. Framework for the construction and validation of the nonstationary standardised streamflow index (NSSI) proposed in this study.

Fig. 3. Monthly (a) precipitation and (b) streamflow series; (c)-(f) Double cumulative curves of annual precipitation and streamflow for the four stations; (g)-(j) Temporal evolution of the reservoir index (RI) and 3-month cumulative streamflow series in June for the four stations ('*' indicates a highly altered streamflow regime).

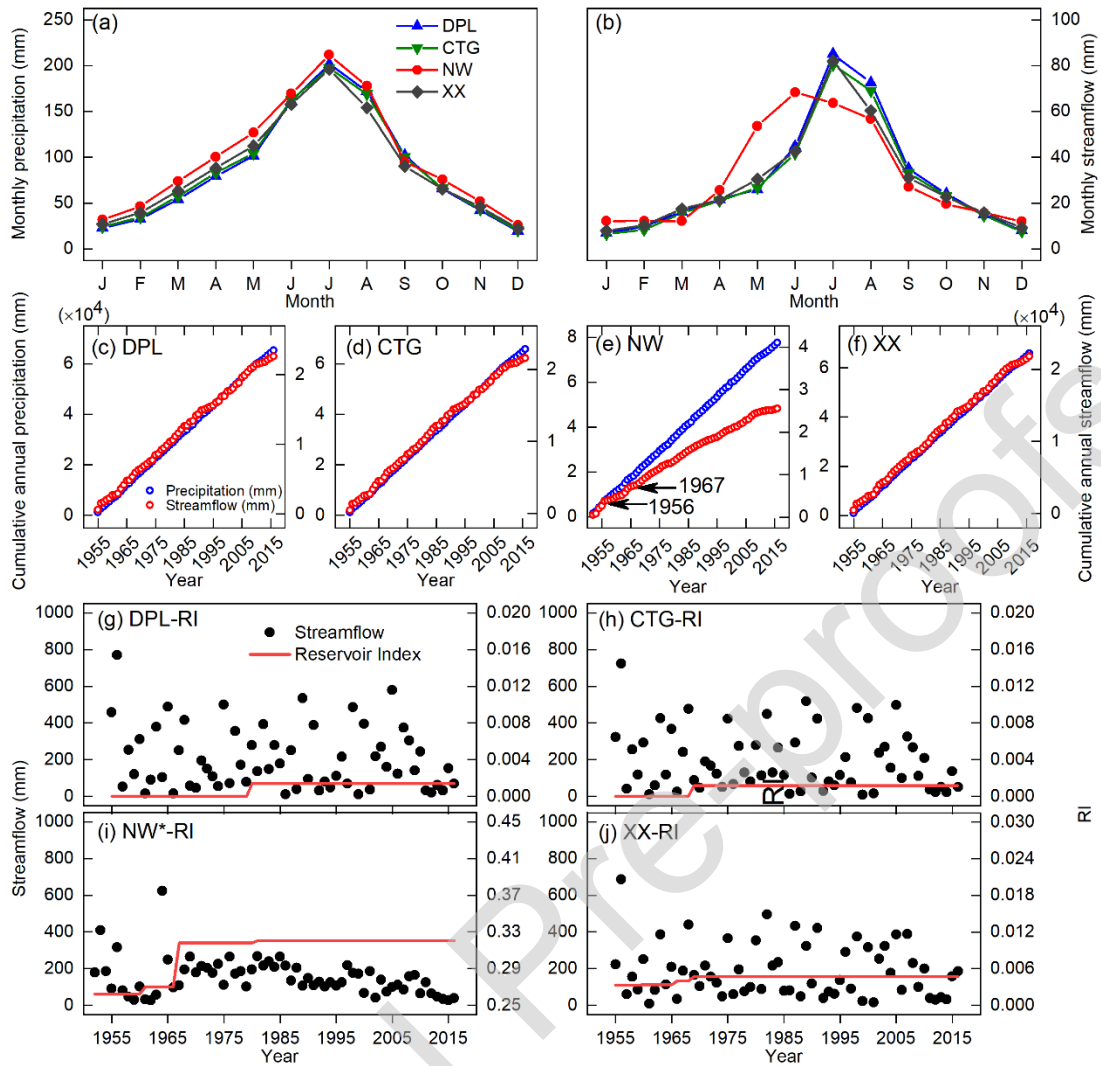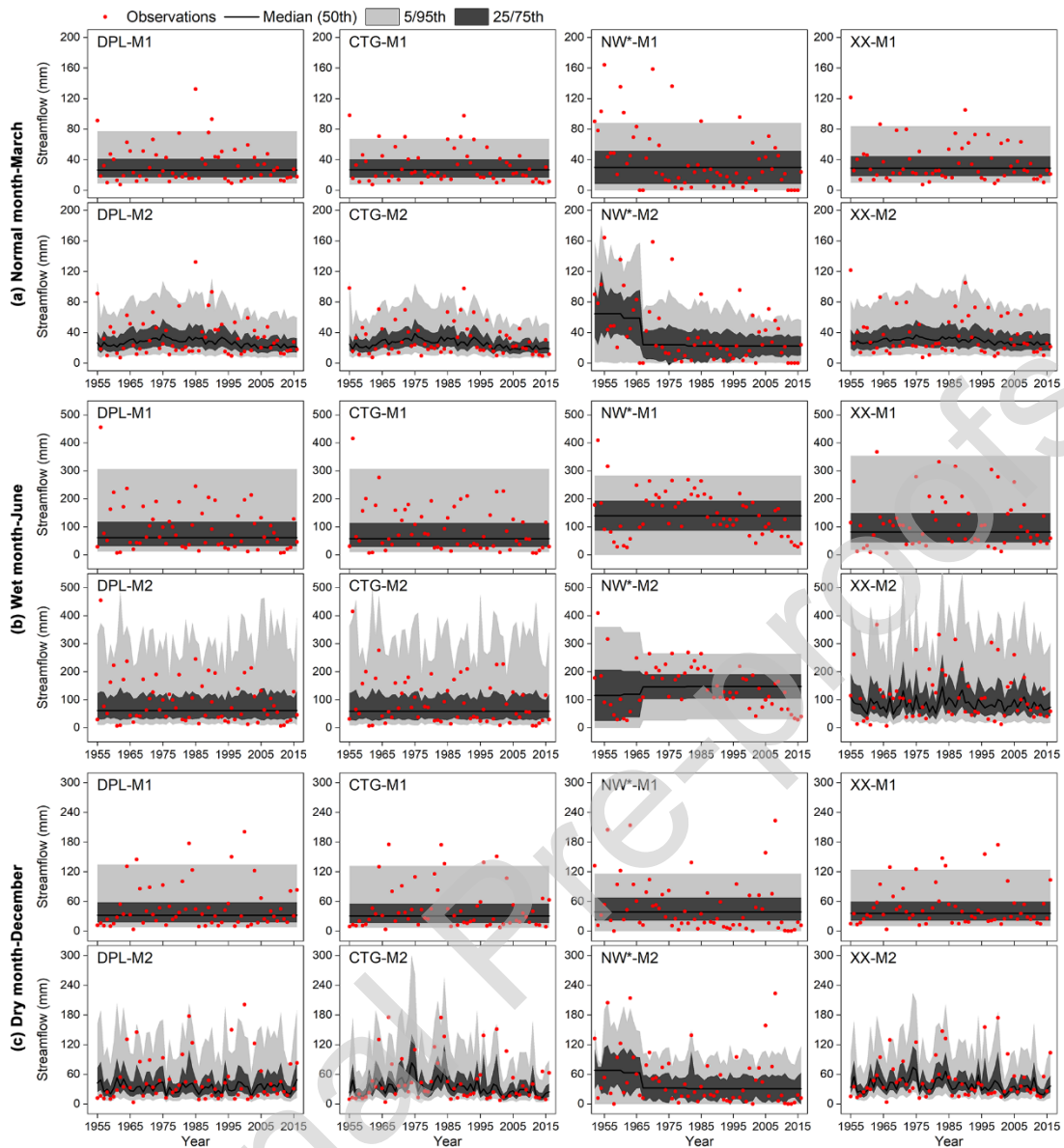**Fig. 4.** Centile curves plots for modelling 3-month cumulative streamflow at the four stations with a stationary model (M1) and nonstationary model (M2) during (a) normal month (March), (b) wet month (June), and (c) dry month (December). '*' indicates a highly altered flow regime. The red points are the observed streamflow series; the blank line is the median (50% centile curve); the dark-grey region represents the area between the 25% and 75% centile curves; and the light-grey region represents the area between the 5% and 95% centile curves.
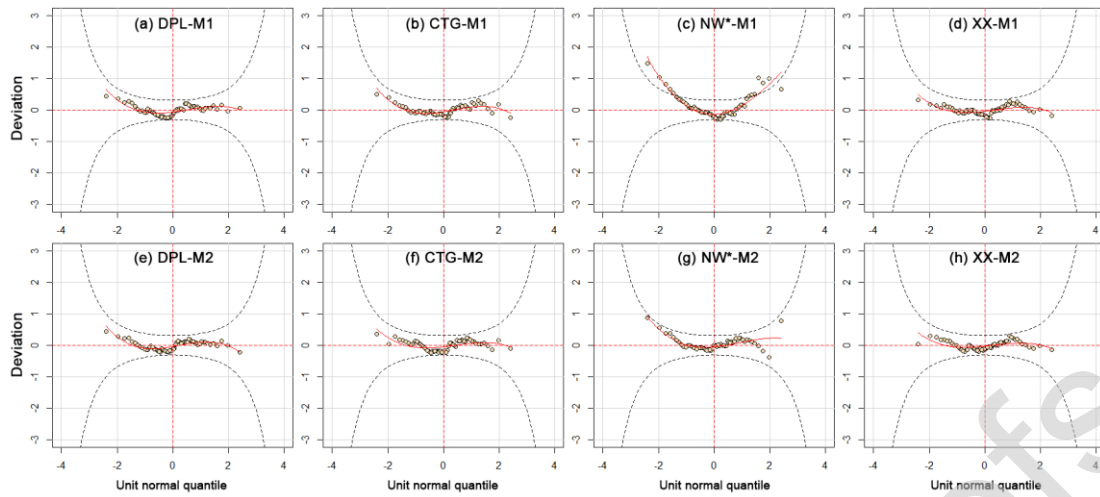
Fig. 5. Worm plots of residuals of the optimal M1 and M2 models for observed streamflow (3-month cumulative streamflow series in March) at the four stations. '*' indicates a highly altered flow regime. The two black dotted lines correspond to the 95% confidence limits. For a good fit, the data points should be aligned preferably along the red solid line but within the two dashed black lines.
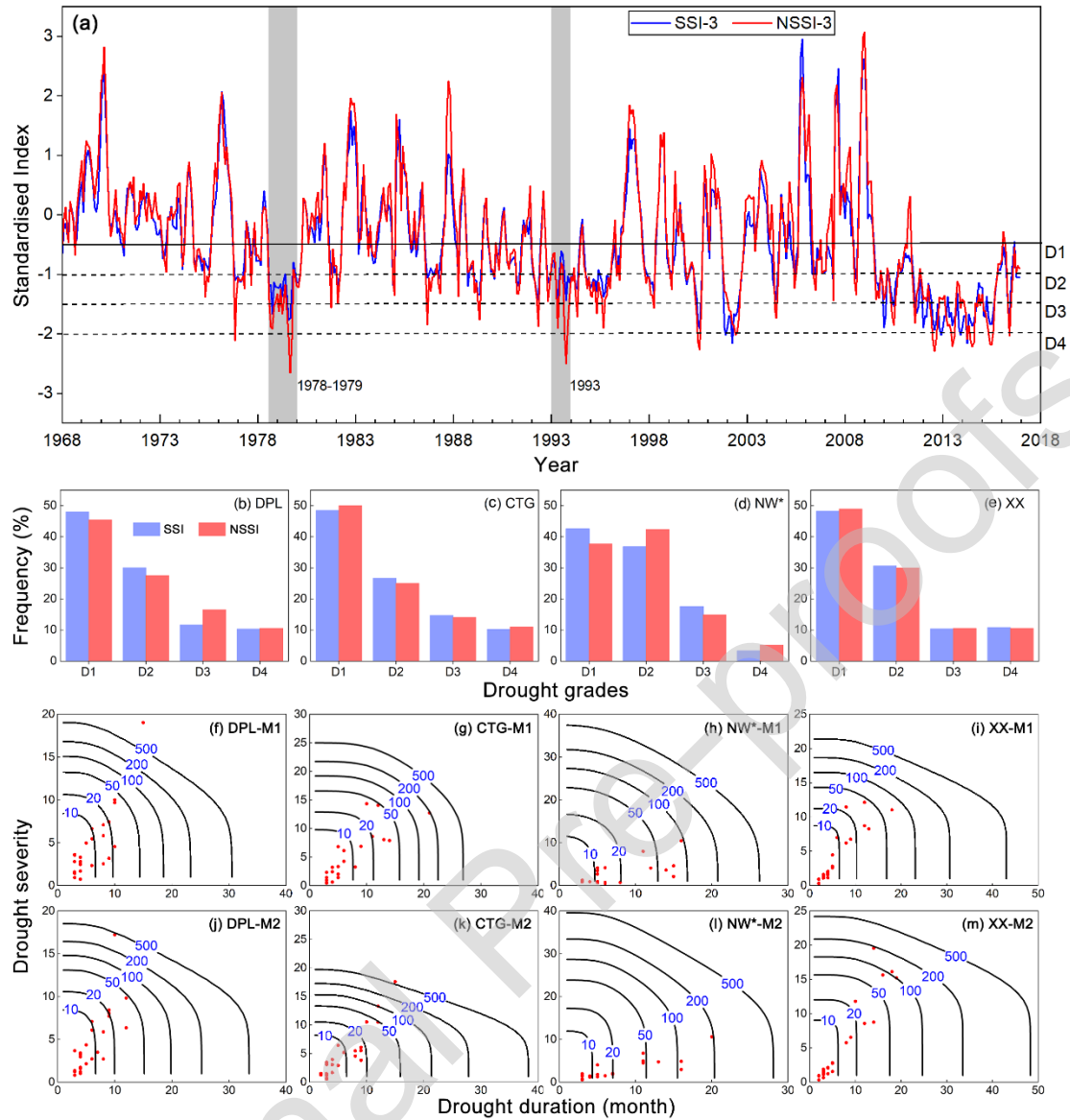
Fig. 6. (a) Temporal series of the standardised streamflow index (SSI) and the nonstationary standardised streamflow index (NSSI) over a 3-month scale at the NW station (the gray shadow bars indicate the hydrological drought events of 1978–1979 and 1993, respectively); (b)-(e) Frequencies of different drought grades (D1–D4) obtained from SSI-3 and NSSI-3 of the four stations; (f)-(m) Joint return periods of hydrological drought duration and severity obtained from the SSI-3 (i.e., M1) and the NSSI-3 (i.e., M2) for the four stations. '*' indicates a highly altered flow regime and red dots indicate the observed hydrological drought events.

Table 1. Results of the trend and change point test of annual precipitation and streamflow for the four stations in the Xixian Basin.

Station	MMK trend test (Z values)		Heuristic segmentation test for change point	
	Precipitation	Streamflow	Precipitation	Streamflow
DPL	–0.92↓	–1.58↓	—	—
CTG	–0.69↓	–1.63↓	—	—
NW	–0.26↓	**–2.16***↓	—	**1956*, 1967***
XX	–0.54↓	–1.48↓	—	—

Notes: '*' with bold values denotes significance at the 95% confidence level. '↑' and '↓' indicate upward and downward trends, respectively.

Table 2. Summary of the significant climate indices for each month of a year at the CTG station.

Month	Climate index						Month	Climate index					
Jan	***$ENSO_{11}$***	NAO_6	AO_6	NPO_1	PDO_{11}	***AMO_1***	Jul	$ENSO_6$	***NAO_{11}***	***AO_5***	NPO_5	PDO_5	***AMO_7***
	0.18	–0.12	–0.14	–0.09	0.13	***–0.28***		0.13	***0.18***	***–0.21***	0.16	0.12	***–0.23***
Feb	***$ENSO_{12}$***	NAO_7	AO_{12}	NPO_5	PDO_{12}	***AMO_2***	Aug	***$ENSO_7$***	NAO_8	AO_6	NPO_6	***PDO_6***	AMO_8
	0.18	–0.12	–0.12	–0.10	0.13	***–0.29***		***0.19***	0.14	–0.14	0.14	***0.18***	–0.24
Mar	$ENSO_3$	NAO_8	AO_1	***NPO_7***	PDO_{11}	***AMO_4***	Sep	***$ENSO_8$***	NAO_6	AO_7	NPO_7	***PDO_7***	AMO_9
	–0.14	–0.10	0.10	***–0.18***	–0.11	***–0.29***		***0.20***	0.16	–0.11	0.11	***0.23***	–0.25
Apr	$ENSO_4$	NAO_8	AO_9	***NPO_7***	PDO_0	AMO_5	Oct	***$ENSO_8$***	NAO_{10}	***AO_0***	***NPO_4***	PDO_8	AMO_{10}
	–0.11	–0.14	–0.09	***–0.22***	–0.14	***–0.28***		***0.20***	0.10	***0.20***	***0.21***	0.24	–0.27
May	$ENSO_5$	NAO_2	AO_1	NPO_5	PDO_1	***AMO_6***	Nov	***$ENSO_9$***	NAO_{12}	AO_4	***NPO_9***	***PDO_9***	***AMO_{11}***
	–0.10	0.13	0.09	–0.14	–0.16	***–0.23***		***0.18***	–0.10	–0.10	***0.17***	***0.19***	***–0.24***
Jun	$ENSO_{12}$	NAO_9	***AO_4***	***NPO_6***	PDO_0	***AMO_6***	Dec	***$ENSO_{10}$***	NAO_3	AO_5	***NPO_0***	PDO_{10}	***AMO_0***
	–0.11	0.13	***–0.18***	***–0.18***	–0.14	***–0.21***		***0.19***	–0.12	–0.09	***–0.18***	0.13	***–0.24***

Notes: Subscript numbers represent the lead times between each climate index and the corresponding month's streamflow. The numbers listed below each climate index are the Kendall correlation coefficients. The climate index with correlation coefficient greater than 95% confidence level is expressed in bold and italics.

Table 3. Summary of the assessment criteria values (GD, AIC, and BIC) for the optimal M1 and M2 models at the NW station and its selected covariate for μ and σ in the optimal M2 model. RI refers to reservoir index and ct refers to a parameter that is independent of the covariates (i.e., constant).

Month	GD		AIC		BIC		The optimal M2 model	
	M1	M2	M1	M2	M1	M2	μ	σ
Jan	619	609	623	617	627	606	RI	RI
Feb	596	585	600	595	604	486	RI	RI, PDO_{11}
Mar	622	604	626	614	630	604	RI	RI, AMO_4
Apr	649	622	653	636	658	631	RI, AMO_5	RI, AMO_5, NPO_8
May	703	678	707	688	712	688	AMO_6	RI, AMO_6
Jun	729	720	733	728	738	717	RI	RI
Jul	750	741	754	749	758	727	RI	RI
Aug	742	732	746	740	750	729	RI	RI
Sep	739	716	743	724	747	722	ct	RI, AMO_{10}
Oct	719	698	723	708	727	698	ct	RI, AO_0, AMO_{11}
Nov	699	680	703	690	707	681	ct	RI, NPO_0, AMO_{12}
Dec	658	646	662	656	666	636	RI	RI, NPO_0

Table 4. Summary of the optimal M1 and M2 models for the four hydrological stations.

Station	Distribution		GD		AIC		BIC	
	M1	M2	M1	M2	M1	M2	M1	M2
DPL	LOGNO	LOGNO	641	627	645	623	650	629
CTG	LOGNO	LOGNO	637	619	641	626	645	623
NW	LO	LO	685	659	689	669	694	669
XX	LOGNO	LOGNO	636	614	640	619	644	624

Notes: LOGNO and LO represent the Lognormal and Logistic distributions, respectively.